Nitrogen-Doped Amorphous Zn-Carbon Multichannel Fibers for Stable Lithium Metal Anodes

*Yongjin Fang, Yinxiang Zeng, Qi Jin, Xue Feng Lu, Deyan Luan, Xitian Zhang, and Xiong Wen (David) Lou**

[*] Q. Jin, Prof X. T. Zhang
School of Physics and Electronic Engineering, Harbin Normal University, Harbin 150025, People's Republic of China

Dr. Y. J. Fang, Dr. Y. X. Zeng, Dr. X. F. Lu, Dr. D. Y. Luan, Prof. X. W. Lou
School of Chemical and Biomedical Engineering, Nanyang Technological University, 62 Nanyang Drive, Singapore 637459, Singapore
Email: xwlou@ntu.edu.sg; Webpage: https://personal.ntu.edu.sg/xwlou/

Abstract

Lithium metal has drawn wide attention as a competitive anode candidate for next-generation high energy density rechargeable batteries. However, the application of lithium metal anodes for practical batteries is still impeded by safety issues and low Coulombic efficiency caused mainly by the uncontrollable growth of lithium dendrites. Herein, two types of free-standing nitrogen-doped amorphous Zn-carbon multichannel fibers are synthesized as multifunctional hosts for lithium accommodation. The three-dimensional (3D) macroporous structures endow effectively reduced local current density, and the lithiophilic nitrogen-doped carbon and functional Zn nanoparticles served as preferred deposition sites with low nucleation barriers to guide uniform lithium deposition. As a result, the developed anodes exhibit remarkable electrochemical properties in terms of high Coulombic efficiency for more than 500 cycles at various current densities from 1 to 5 mA cm^{-2}, and symmetric cells show long-term cycling duration over 2000 h. Moreover, full cells based on the developed anode and a $LiFePO_4$ cathode also demonstrate superior rate capability and stable cycle life.

Keywords: Zn nanoparticles, macroporous carbon fibers, hollow nanostructures, lithiophilic sites, lithium metal anodes

The ever-growing demand for high-energy and high-power rechargeable batteries to electrify transportation and grid-scale energy storage systems has continuously spurred the battery community to explore advanced electrode materials.[1-3] Metallic lithium has been an attractive choice as the ultimate anode owing to its high theoretical capacity (3861 mAh g^{-1}), very low electrochemical potential (-3.04 V versus standard hydrogen electrode), and small gravimetric density (0.534 g cm^{-3}).[4-8] Unfortunately, the practical application of Li metal anodes (LMAs) has not been realized due to the structural and interfacial instability issues induced by the uncontrollable growth of Li dendrites during repeated electrochemical cycling processes.[9-11] Extensive efforts have been recently made to regulate the Li deposition/dissolution properties for stable LMAs, including developing compatible electrolytes,[12-16] engineering rationally designed three-dimensional (3D) scaffolds for Li accommodation,[17-20] and constructing artificial solid-electrolyte interphase (SEI) layers.[21-24] Among these approaches, 3D host nanostructures for LMAs have shown outstanding electrochemical properties because of the largely decreased local current density and accommodated huge volume variation during Li accommodation/extraction.[25, 26] However, restricted by the poor absorbing ability for Li^+ ions, common 3D matrixes can hardly regulate the Li^+ ion concentration close to the electrode/electrolyte interface, resulting in limited cycle life and moderate rate capability.

As an effective strategy, constructing functional species decorated host structures has been reported to show enhanced cyclability for LMAs.[27, 28] Yan et al. investigated the Li deposition properties on different substrates and confirmed that Li metal can selectively deposit on Zn, Ag, and Au nanoseeds owing to their high solubility in Li, achieving ultralow or zero nucleation barriers for subsequent Li deposition.[29] More specifically, from the Zn-Li binary phase diagram (Figure S1a, see Supporting Information), Zn can easily react with Li to form a series of Li_xZn_y alloy phases at room temperature. During the Li deposition process, nanosized Zn will first dissolve into Li to form a solid solution surface layer with a high lithium diffusion coefficient, which can serve as a buffer layer with eliminated nucleation barriers for the subsequent Li deposition under the layer.[29-31] In

contrast, such a solid solution feature does not exist when Cu is used as the substrates (Figure S1b). Later on, the Zn- and ZnO-based nanoparticles are further proven as efficient heterogeneous nucleation sites to achieve stable Li plating/stripping properties.[32-34] On the other hand, owing to the fascinating properties of high specific surface area, good flexibility and distinct absorbability, porous carbon fibers have been demonstrated to enable homogenous Li deposition and enhance SEI layer stability.[26, 35, 36] The 3D carbon matrix can effectively decrease local current density, accommodate the volume change, and release compressive stress, thus successfully suppressing the growth of Li dendrites. Furthermore, by employing heteroatom-doped carbon materials as the lithium host, the Li deposition properties can be effectively regulated due to the reduced barrier for heterogenous Li nucleation on the lithiophilic heteroatom-doped carbon sites, hence resulting in dendrite-free Li deposition and prolonged cycling.[37, 38] Based on the above considerations, it would be of great significance by integrating these merits into one alliance to design macroporous carbon fibers decorated with functional sites to boost their potential for high-performance LMAs.

Herein, we present the elaborate design and construction of a 3D host consisting of carbon cages (CC) decorated nitrogen-doped amorphous Zn-carbon multichannel fibers (denoted as CC-Zn-CMFs) for stable LMAs. The structural and compositional design has multifold advantages: (1) the 3D electronically conductive hierarchical carbon fibers with a large surface area can efficiently promote the transfer of electron and decrease the local current density; (2) the macroporous structures with nanocages on multichannel carbon fibers can accommodate the huge volume change during long-term electrochemical cycling; (3) lithiophilic nitrogen-doped carbon and functional Zn nanoparticles show strong anchoring effect for Li^+ ions, endowing targeted Li deposition on the hierarchical porous carbon; (4) the stretchable and robust scaffold can accommodate the compressive stress during repeated plating/stripping processes. Benefitting from these integrated advantages, the CC-Zn-CMFs based anode manifests remarkable electrochemical properties in both half and full cells.

The synthesis process of the CC-Zn-CMFs is schematically displayed in **Figure 1**a. First, a mixture of $Zn(Ac)_2$, polystyrene (PS), and polyacrylonitrile (PAN) in N,N-dimethylformamide is manufactured into PAN/PS-$Zn(Ac)_2$ fibers by electrospinning. Afterward, a layer of zinc-based zeolitic imidazolate framework (ZIF-8) nanoparticles is grown on the surface of the PAN/PS-$Zn(Ac)_2$ fibers after immersing the PAN/PS-$Zn(Ac)_2$ fibers in 2-methylimidazole/ethanol solution for 24 h. During a subsequent heat treatment in N_2, the ZIF-8@PAN/PS-$Zn(Ac)_2$ fibers are easily converted to CC-Zn-CMFs. Both the structure and composition of anticipated CC-Zn-CMFs can be achieved through the elaborately designed recipe. As expected, the CC-Zn-CMFs host demonstrates remarkable electrochemical properties for LMAs.

Field-emission scanning electron microscopy (FESEM) images reveal that the PAN/PS-$Zn(Ac)_2$ product has a one-dimensional fiber morphology with diameters in the range of 1.5-2.0 μm (Figure 1b and Figure S2a and b). The surface of the fibers is very smooth (Figure 1c and d, and Figure S2c). After being immersed in a 2-methylimidazole ethanol solution, the $Zn(Ac)_2$ in the PAN/PS-$Zn(Ac)_2$ fibers can react with 2-methylimidazole to form a shell of ZIF-8 nanocrystals on the PAN/PS-$Zn(Ac)_2$ fibers. Typical FESEM images (Figure 1e and Figure S3a) of the obtained sample shows that the fiber morphology is well maintained but the surface becomes very rough. A closer observation discloses that the surface of the fiber is coated with close-packed nanoparticles (Figure 1f and Figure S3b). Transmission electron microscopy (TEM) images further confirm the core-shell structures (Figure 1g and Figure S3c). The X-ray diffraction (XRD) pattern of the composite shows the typical diffraction peaks of the ZIF-8 (Figure S4). All these results elucidate the successful formation of ZIF-8 nanoparticles on the PAN/PS-$Zn(Ac)_2$ fibers.

Afterward, the ZIF-8@PAN/PS-$Zn(Ac)_2$ fibers are carbonized at 600ºC in N_2 to form the CC-Zn-CMFs. FESEM images show that the CC-Zn-CMFs inherit the hierarchical fiber structures (**Figure 2**a and Figure S5a), and the surface remains very rough (Figure 2b,c and Figure S5b). Expectedly, the cross-section images directly show the unique multichannel structures (Figure 2d and

Figure S5c), which are related to the decomposition of the PS component during the carbonization process.[39] The highly paralleled channels are uniformly aligned along the fibers (Figure 2e and Figure S5d). Interestingly, an enlarged examination shows that there are nanocages compactly anchored on the surface of the hollow fiber (Figure 2f). The formation of the nanocages is attributed to the fast pyrolysis of ZIF-8 to generate carbon and Zn species at elevated temperature.[40, 41] No discernible lattice fringe can be observed from the HRTEM observation (Figure 2g), revealing the amorphous character of the CC-Zn-CMFs. The amorphous structure has been further confirmed by XRD characterization (Figure S6). This result is consistent with reported results as Zn/carbon materials tend to form the amorphous state even at high carbonization temperatures.[40, 42] Elemental mappings of an individual fiber illustrate that Zn, C, and N elements are homogeneously dispersed throughout the hollow fiber (Figure 2h). And energy-dispersive X-ray spectroscope (EDX) result (Figure S7) confirms the presence of the Zn element in the obtained product. To show the effect of these decorated carbon nanocages on electrochemical properties of the product, the other sample without carbon nanocages, that is, nitrogen-doped amorphous Zn-carbon multichannel fibers (denoted as Zn-CMFs), is easily prepared by direct carbonization of the PAN/PS-$Zn(Ac)_2$ fibers. The Zn-CMFs show similar multichannel fiber structures with a smooth surface (Figure 2i-l) and are also amorphous (Figure S6).

Raman spectra show the typical D and G bands of carbon in both Zn-CMFs and CC-Zn-CMFs (Figure 2m).[43, 44] As disclosed by thermogravimetric analysis result, the weight contents of Zn nanoparticles in the Zn-CMFs and CC-Zn-CMFs are determined to be about 23.9 and 20.5 wt%, respectively (Figure 2n). Nitrogen adsorption/desorption isotherms reveal that the CC-Zn-CMFs composite has a mesoporous structure with a higher Brunauer-Emmett-Teller (BET) surface area (74.7 $m^2 g^{-1}$) compared to the Zn-CMFs (61.8 $m^2 g^{-1}$) (Fig. 3o). The elemental composition (i.e., Zn, N, and C) of the CC-Zn-CMFs is examined by X-ray photoelectron spectroscopy (XPS) (Figure S8).

Figure 3a shows the typical plating/stripping voltage curves of the CC-Zn-CMFs electrode. During the discharge process, the voltage gradually decreases to zero and the nucleated Li metal begins to grow on the CC-Zn-CMFs. The electrode shows negligible morphology change when the plating capacity reaches 2 mAh cm^{-2} (Figure 3c), and the multichannel structure becomes inconspicuous (Figure S9), implying that Li is deposited mainly in the hollow interspace of the porous carbon fibers.[29, 36, 45] No Li dendrites are discerned when the deposition capacity of lithium is as high as 4 mAh cm^{-2} (Figure 3d). With the plating capacity further increased to 6 mAh cm^{-2}, the electrode appears less porous, indicating the lithium deposition occurs in the space between the fibers (Figure 3e). Impressively, the surface of the electrode becomes smooth with the fibers buried in the plated Li when the areal capacity increases to a high level of 10 mAh cm^{-2} (Figure 3f). And no dendric or mossy Li is observed in the enlarged observations of the electrodes (Figure S10). In vast contrast, uncontrollable Li dendrites grow wildly on bare Cu (*b*-Cu) with only a small plated Li capacity of 2 mAh cm^{-2} (Figure S11). In the subsequent charging procedure of the CC-Zn-CMFs-Li, Li is gradually stripped and the free space between the fibers is reversibly recovered (Figure 3g, h). Notably, the 3D structure of the CC-Zn-CMFs is well preserved without discernible Li residue after being charged to 1.5 V (Figure 3i), indicating the good structural integrity of the 3D host. Based on the morphological evolution of CC-Zn-CMFs during Li plating, the potential Li deposition process on CC-Zn-CMFs is schematically displayed as the inset in Figure 3a. Li deposition initiates in the hollow interspace of the fibers because of the high curvature on the inner wall.[45] With further Li plating, Li will deposit on the surface of the fibers and grow in the space among the fibers, which can effectively prevent the outward dendrite growth.

The electrochemical properties of the obtained electrodes are first evaluated by testing the Coulombic efficiency (CE) during repeated Li plating/stripping processes. **Figure 4**a presents the CE of the *b*-Cu, Zn-CMFs, and CC-Zn-CMFs electrodes at current densities from 1 to 5 mA cm^{-2} with a deposition capacity of 1 mAh cm^{-2}. The CC-Zn-CMFs electrode exhibits a stable CE for an ultralong

cycle life of 800 cycles at 1 mA cm^{-2}. When the current density is elevated to high values of 2, 3, and 5 mA cm^{-2}, a stable cycle life of above 500 cycles can also be achieved. Notably, the Zn-CMFs electrodes also show relatively stable cycle life at different current densities, while the CE of *b*-Cu electrodes fades rapidly after 70 cycles. Besides, the selected Li plating/striping voltage profiles further validate the stable cycling performance of the CC-Zn-CMFs electrodes (Figure 4b), which show much smaller overpotential compared to the *b*-Cu electrode (Figure S12).

Li//Li symmetrical cells are assembled to investigate the cycling stability of the electrodes. The rate capability of the CC-Zn-CMFs-Li//CC-Zn-CMFs-Li symmetrical cell is tested at different current densities ranging from 0.5 to 10 mA cm^{-2} with a fixed Li deposition capacity of 2 mAh cm^{-2} (Figure 4c). Impressively, the CC-Zn-CMFs-Li anode shows small and steady overpotentials at different current densities. Specifically, a small overpotential of 20 mV at 0.5 mAh cm^{-2} is observed. Even at an ultrahigh current density of 10 mA cm^{-2}, a relatively low voltage hysteresis of 220 mV can still be achieved. Comparatively, the *b*-Cu-Li possesses much larger overpotentials at different current densities (Figures S13 and S14). Moreover, the CC-Zn-CMFs-Li anode also exhibits excellent cycling stability. The lifespan of the symmetric cell is impressively extended to 2000 h at 1 mA cm^{-2} by the CC-Zn-CMFs-Li anode, accompanied with an ultralow overpotential of about 30 mV which is much lower than that of Zn-CMFs-Li (Figure 4d). As a comparison, the *b*-Cu-Li anode exhibits a sudden voltage drop around 150 h indicating an internal short circuit, followed by some very wide overpotential. These outstanding electrochemical properties of the CC-Zn-CMFs electrodes can be attributed to the unique hollow configuration and synergistic effect of the functional Zn nanoparticles anchored on macroporous nitrogen-doped carbon nanofibers. More specifically, the interconnected electronically conductive 3D network offers a smooth pathway for electrons and effectively minimizes the local current density. The favorable flexibility and hierarchical hollow nanostructures can buffer the volume change and release the compressive stress during repeated Li plating/stripping. The lithiophilic nitrogen-doped carbon enables an ultralow barrier for guiding homogeneous Li

nucleation and growth. And the Zn nanoparticles will dissolve into Li via the solid-solution reaction to form the Li_xZn_y alloy interface layer, which offers a high Li atom diffusion coefficient and ultralow nucleation barrier to achieve stable cycling performance with high CE.

As an assessment of the applicability of CC-Zn-CMFs for lithium batteries, coin-type CC-Zn-CMFs-Li//$LiFePO_4$ (LFP) full cells are assembled, and their electrochemical characteristics are examined. The CC-Zn-CMFs-Li//LFP cell exhibits a remarkable rate capability at different current rates. Accordingly, the full cells can output an average reversible capacity of 151, 150, 146, 140, 129, and 104 mAh g^{-1} at 0.1, 0.2, 0.5, 1, 2, and 5 C, respectively (**Figure 5**a). Of note, the CC-Zn-CMFs-Li//LFP cell manifests small polarization even the current rate is increased to 5 C (Figure 5b). Moreover, the CC-Zn-CMFs-Li//LFP cell also shows good cyclability. An ultrastable cycle life of 200 cycles without obvious capacity decay can be observed (Figure 5c). In comparison, the capacity of the *b*-Cu-Li//LFP cell fades rapidly after 70 cycles, while the Zn-CMFs-Li//LFP cell also shows enhanced cycle life. These results suggest the feasibility of CC-Zn-CMFs for practical batteries.

In summary, we have proposed the delicate design and fabrication of carbon cages decorated nitrogen-doped amorphous Zn-carbon multichannel fibers (CC-Zn-CMFs) as a lithium host for lithium metal anodes. The 3D macroporous fiber structure can buffer the huge volume change during long-term Li plating/stripping processes, and the lithiophilic nitrogen-doped carbon and functional Zn nanoparticles can effectively control the nucleation and growth of Li due to ultralow overpotentials. As a result, the lithium metal anodes based on CC-Zn-CMFs exhibit high Coulombic efficiency for more than 500 cycles at current densities ranging from 1 to 5 mA cm^{-2}. The symmetric cells based on CC-Zn-CMFs-Li also demonstrate outstanding rate capability and long duration for 2000 h. Furthermore, the CC-Zn-CMFs-Li//LFP full cell manifests significantly improved rate capability and stable cycle life. This work may inspire further potentials for the design and synthesis of efficient functional Li hosts for stable lithium metal anodes.

Acknowledgments

X.W.L. acknowledges the funding support from the National Research Foundation (NRF) of Singapore via the NRF investigatorship (NRF-NRFI2016-04), and Ministry of Education of Singapore via the AcRF Tier-1 grant (RG3/20). X.T.Z. acknowledges the funding support from National Natural Science Foundation of China (51772069).

References

[1] M. Armand, J. M. Tarascon, *Nature* **2008**, *451*, 652.

[2] Y. Cao, M. Li, J. Lu, J. Liu, K. Amine, *Nat. Nanotechnol.* **2019**, *14*, 200.

[3] J. Liu, Z. Bao, Y. Cui, E. J. Dufek, J. B. Goodenough, P. Khalifah, Q. Li, B. Y. Liaw, P. Liu, A. Manthiram, Y. S. Meng, V. R. Subramanian, M. F. Toney, V. V. Viswanathan, M. S. Whittingham, J. Xiao, W. Xu, J. Yang, X.-Q. Yang, J.-G. Zhang, *Nat. Energy* **2019**, *4*, 180.

[4] J. Xiao, *Science* **2019**, *366*, 426.

[5] C. Fang, J. Li, M. Zhang, Y. Zhang, F. Yang, J. Z. Lee, M.-H. Lee, J. Alvarado, M. A. Schroeder, Y. Yang, B. Lu, N. Williams, M. Ceja, L. Yang, M. Cai, J. Gu, K. Xu, X. Wang, Y. S. Meng, *Nature* **2019**, *572*, 511.

[6] X.-B. Cheng, R. Zhang, C.-Z. Zhao, Q. Zhang, *Chem. Rev.* **2017**, *117*, 10403.

[7] P. Albertus, S. Babinec, S. Litzelman, A. Newman, *Nat. Energy* **2018**, *3*, 16.

[8] L. Li, S. Basu, Y. Wang, Z. Chen, P. Hundekar, B. Wang, J. Shi, Y. Shi, S. Narayanan, N. Koratkar, *Science* **2018**, *359*, 1513.

[9] D. Lin, Y. Liu, Y. Cui, *Nat. Nanotechnol.* **2017**, *12*, 194.

[10] M. D. Tikekar, S. Choudhury, Z. Tu, L. A. Archer, *Nat. Energy* **2016**, *1*, 16114.

[11] M. J. Zachman, Z. Tu, S. Choudhury, L. A. Archer, L. F. Kourkoutis, *Nature* **2018**, *560*, 345.

[12] L. Xiao, Z. Zeng, X. Liu, Y. Fang, X. Jiang, Y. Shao, L. Zhuang, X. Ai, H. Yang, Y. Cao, J. Liu, *ACS Energy Lett.* **2019**, *4*, 483.

[13] Y. Lu, Z. Tu, L. A. Archer, *Nat. Mater.* **2014**, *13*, 961.

[14] X. Cao, X. Ren, L. Zou, M. H. Engelhard, W. Huang, H. Wang, B. E. Matthews, H. Lee, C. Niu, B. W. Arey, Y. Cui, C. Wang, J. Xiao, J. Liu, W. Xu, J.-G. Zhang, *Nat. Energy* **2019**, *4*, 796.

[15] X. Han, Y. Gong, K. Fu, X. He, G. T. Hitz, J. Dai, A. Pearse, B. Liu, H. Wang, G. Rubloff, Y. Mo, V. Thangadurai, E. D. Wachsman, L. Hu, *Nat. Mater.* **2017**, *16*, 572.

[16] X. Ren, P. Gao, L. Zou, S. Jiao, X. Cao, X. Zhang, H. Jia, M. H. Engelhard, B. E. Matthews, H. Wu, H. Lee, C. Niu, C. Wang, B. W. Arey, J. Xiao, J. Liu, J.-G. Zhang, W. Xu, *Proc. Natl. Acad. Sci.* **2020**, *117*, 28603.

[17] C. Zhang, S. Liu, G. Li, C. Zhang, X. Liu, J. Luo, *Adv. Mater.* **2018**, *30*, 1801328.

[18] D. Lin, J. Zhao, J. Sun, H. Yao, Y. Liu, K. Yan, Y. Cui, *Proc. Natl. Acad. Sci.* **2017**, *114*, 4613.

[19] C. Niu, H. Pan, W. Xu, J. Xiao, J.-G. Zhang, L. Luo, C. Wang, D. Mei, J. Meng, X. Wang, Z. Liu, L. Mai, J. Liu, *Nat. Nanotechnol.* **2019**, *14*, 594.

[20] Y. Fang, S. L. Zhang, Z. P. Wu, D. Luan, X. W. Lou, **2021**, submitted.

[21] H. Yuan, J. Nai, H. Tian, Z. Ju, W. Zhang, Y. Liu, X. Tao, X. W. Lou, *Sci. Adv.* **2020**, *6*, eaaz3112.

[22] H. Yuan, J. Nai, Y. Fang, G. Lu, X. Tao, X. W. Lou, *Angew. Chem. Int. Ed.* **2020**, *59*, 15839.

[23] L. Wang, A. Menakath, F. Han, Y. Wang, P. Y. Zavalij, K. J. Gaskell, O. Borodin, D. Iuga, S. P. Brown, C. Wang, K. Xu, B. W. Eichhorn, *Nat. Chem.* **2019**, *11*, 789.

[24] S. Liu, X. Ji, N. Piao, J. Chen, N. Eidson, J. Xu, P. Wang, L. Chen, J. Zhang, T. Deng, S. Hou, T. Jin, H. Wan, J. Li, J. Tu, C. Wang, *Angew. Chem. Int. Ed.* **2020**, DOI: 10.1002/anie.202012005.

[25] T.-T. Zuo, X.-W. Wu, C.-P. Yang, Y.-X. Yin, H. Ye, N.-W. Li, Y.-G. Guo, *Adv. Mater.* **2017**, *29*, 1700389.

[26] K. Yan, B. Sun, P. Munroe, G. Wang, *Energy Storage Mater.* **2018**, *11*, 127.

[27] Y.-G. Lee, S. Fujiki, C. Jung, N. Suzuki, N. Yashiro, R. Omoda, D.-S. Ko, T. Shiratsuchi, T. Sugimoto, S. Ryu, J. H. Ku, T. Watanabe, Y. Park, Y. Aihara, D. Im, I. T. Han, *Nat. Energy* **2020**, *5*, 299.

[28] R. Zhang, X. Chen, X. Shen, X.-Q. Zhang, X.-R. Chen, X.-B. Cheng, C. Yan, C.-Z. Zhao, Q. Zhang, *Joule* **2018**, *2*, 764.

[29] K. Yan, Z. Lu, H.-W. Lee, F. Xiong, P.-C. Hsu, Y. Li, J. Zhao, S. Chu, Y. Cui, *Nat. Energy* **2016**, *1*, 16010.

[30] X. Liang, Q. Pang, I. R. Kochetkov, M. S. Sempere, H. Huang, X. Sun, L. F. Nazar, *Nat. Energy* **2017**, *2*, 17119.

[31] S. Jin, Y. Ye, Y. Niu, Y. Xu, H. Jin, J. Wang, Z. Sun, A. Cao, X. Wu, Y. Luo, H. Ji, L.-J. Wan, *J. Am. Chem. Soc.* **2020**, *142*, 8818.

[32] Y. Liu, D. Lin, Z. Liang, J. Zhao, K. Yan, Y. Cui, *Nat. Commun.* **2016**, *7*, 10992.

[33] Y. Zhang, W. Luo, C. Wang, Y. Li, C. Chen, J. Song, J. Dai, E. M. Hitz, S. Xu, C. Yang, Y. Wang, L. Hu, *Proc. Natl. Acad. Sci.* **2017**, *114*, 3584.

[34] C. Jin, O. Sheng, J. Luo, H. Yuan, C. Fang, W. Zhang, H. Huang, Y. Gan, Y. Xia, C. Liang, J. Zhang, X. Tao, *Nano Energy* **2017**, *37*, 177.

[35] Y. Zhang, C. Wang, G. Pastel, Y. Kuang, H. Xie, Y. Li, B. Liu, W. Luo, C. Chen, L. Hu, *Adv. Energy Mater.* **2018**, *8*, 1800635.

[36] L. Liu, Y.-X. Yin, J.-Y. Li, N.-W. Li, X.-X. Zeng, H. Ye, Y.-G. Guo, L.-J. Wan, *Joule* **2017**, *1*, 563.

[37] R. Zhang, X.-R. Chen, X. Chen, X.-B. Cheng, X.-Q. Zhang, C. Yan, Q. Zhang, *Angew. Chem. Int. Ed.* **2017**, *56*, 7764.

[38] X. Chen, X.-R. Chen, T.-Z. Hou, B.-Q. Li, X.-B. Cheng, R. Zhang, Q. Zhang, *Sci. Adv.* **2019**, *5*, eaau7728.

[39] Z. Li, J. Zhang, Y. Lu, X. W. Lou, *Sci. Adv.* **2018**, *4*, eaat1687.

[40] C. Yan, X. Gu, L. Zhang, Y. Wang, L. Yan, D. Liu, L. Li, P. Dai, X. Zhao, *J. Mater. Chem. A* **2018**, *6*, 17371.

[41] S. Wang, Y. Wang, S. L. Zhang, S.-Q. Zang, X. W. Lou, *Adv. Mater.* **2019**, *31*, 1903404.

[42] Z. Wang, J. Huang, Z. Guo, X. Dong, Y. Liu, Y. Wang, Y. Xia, *Joule* **2019**, *3*, 1289.

[43] Y. Fang, D. Luan, Y. Chen, S. Gao, X. W. Lou, *Angew. Chem. Int. Ed.* **2020**, *59*, 7178.

[44] Y. Fang, J. Zhang, F. Zhong, X. Feng, W. Chen, X. Ai, H. Yang, Y. Cao, *CCS Chem.* **2020**, *2*, 2428.

[45] J. Xiang, Y. Zhao, L. Yuan, C. Chen, Y. Shen, F. Hu, Z. Hao, J. Liu, B. Xu, Y. Huang, *Nano Energy* **2017**, *42*, 262.

Figures and Captions

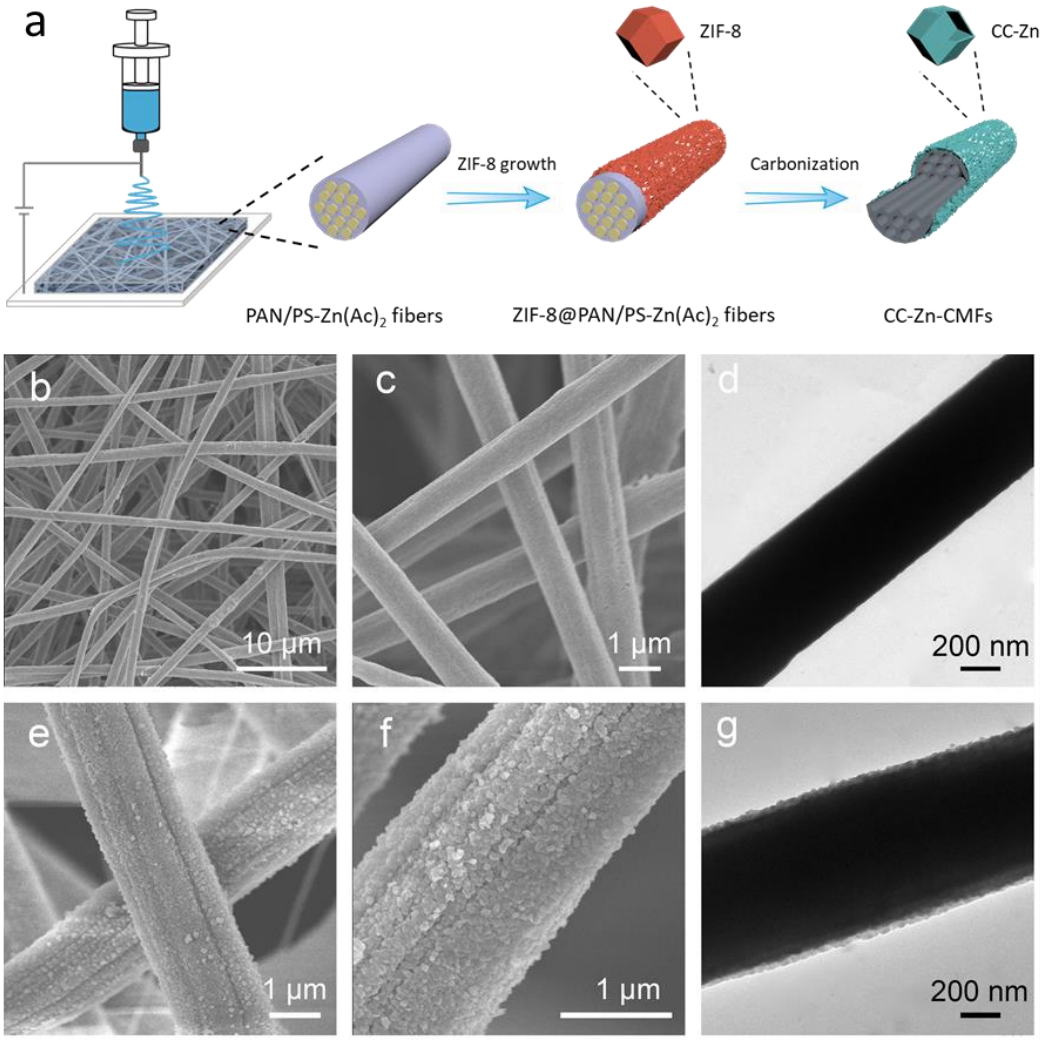

Figure 1. (a) Schematic illustration of the synthesis of CC-Zn-CMFs. (b, c, e, f) FESEM images and (d, g) TEM images of the (b-d) PAN/PS-Zn(Ac)$_2$ fibers and (e-g) ZIF-8@PAN/PS-Zn(Ac)$_2$ fibers.

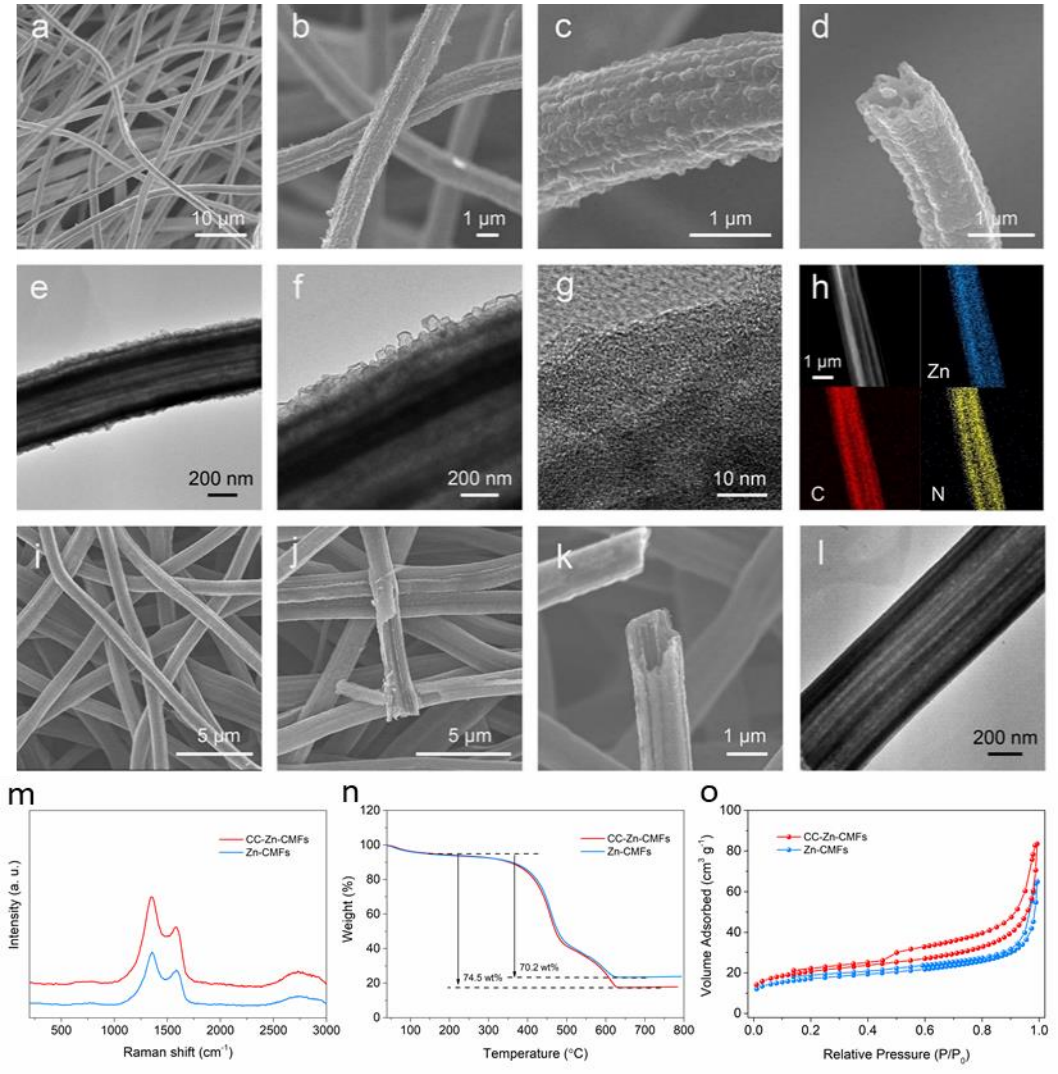

Figure 2. (a-d, i-k) FESEM images, (e, f, l) TEM images, and (g) HRTEM image of (a-g) CC-Zn-CMFs and (i-l) Zn-CMFs. (h) Typical HAADF-STEM image and corresponding elemental mapping images of CC-Zn-CMFs. (m) Raman spectra, (n) thermogravimetric analyses in air at a heating rate of 10ºC min^{-1}, and (o) N_2 adsorption and desorption isotherms of CC-Zn-CMFs and Zn-CMFs.

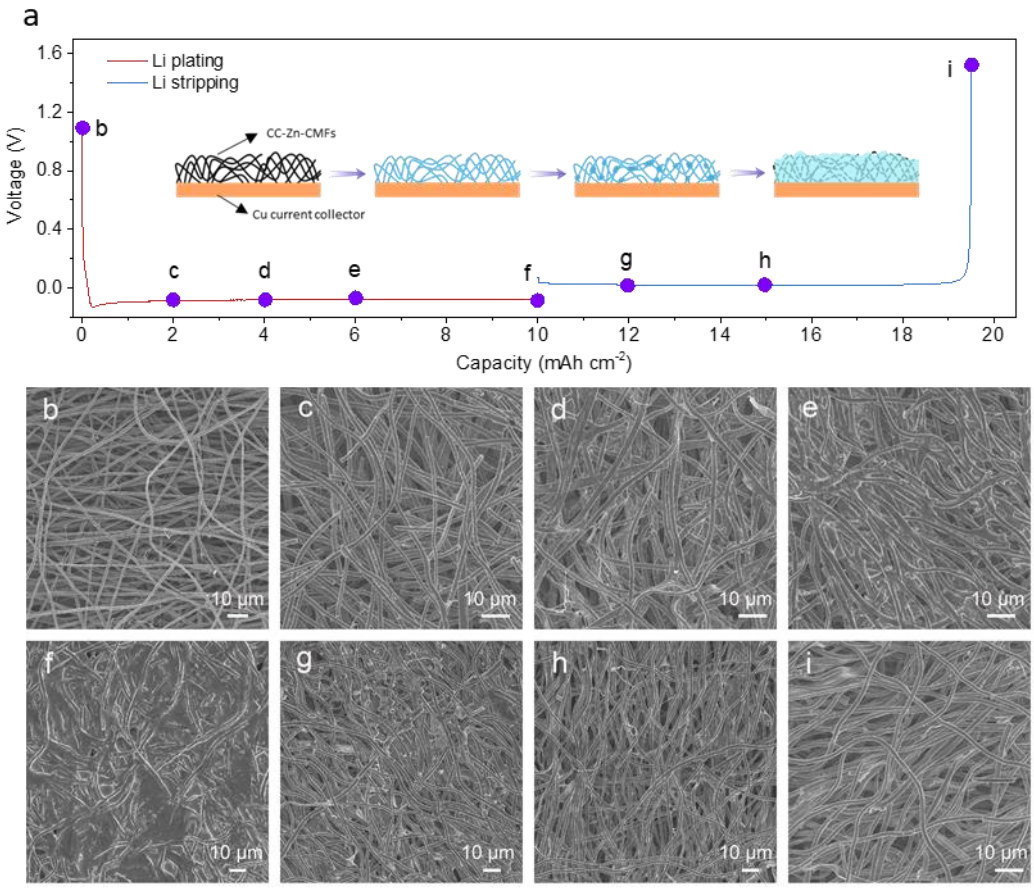

Figure 3. (a) Electrochemical Li plating/stripping curves of the CC-Zn-CMFs electrode at 1 mA cm^{-2} for a capacity of 10 mAh cm^{-2}. (b) FESEM image of the CC-Zn-CMFs electrode. (c-i) FESEM images of CC-Zn-CMFs electrodes after being plated with (c) 2 mAh cm^{-2}, (d) 4 mAh cm^{-2}, (e) 6 mAh cm^{-2}, and (f) 10 mAh cm^{-2} of Li metal; anodes after stripping (g) 2 mAh cm^{-2}, (h) 5 mAh cm^{-2}, and (i) 10 mAh cm^{-2} (i.e., recharged to 1.5 V) from the Li anodes with the CC-Zn-CMFs.

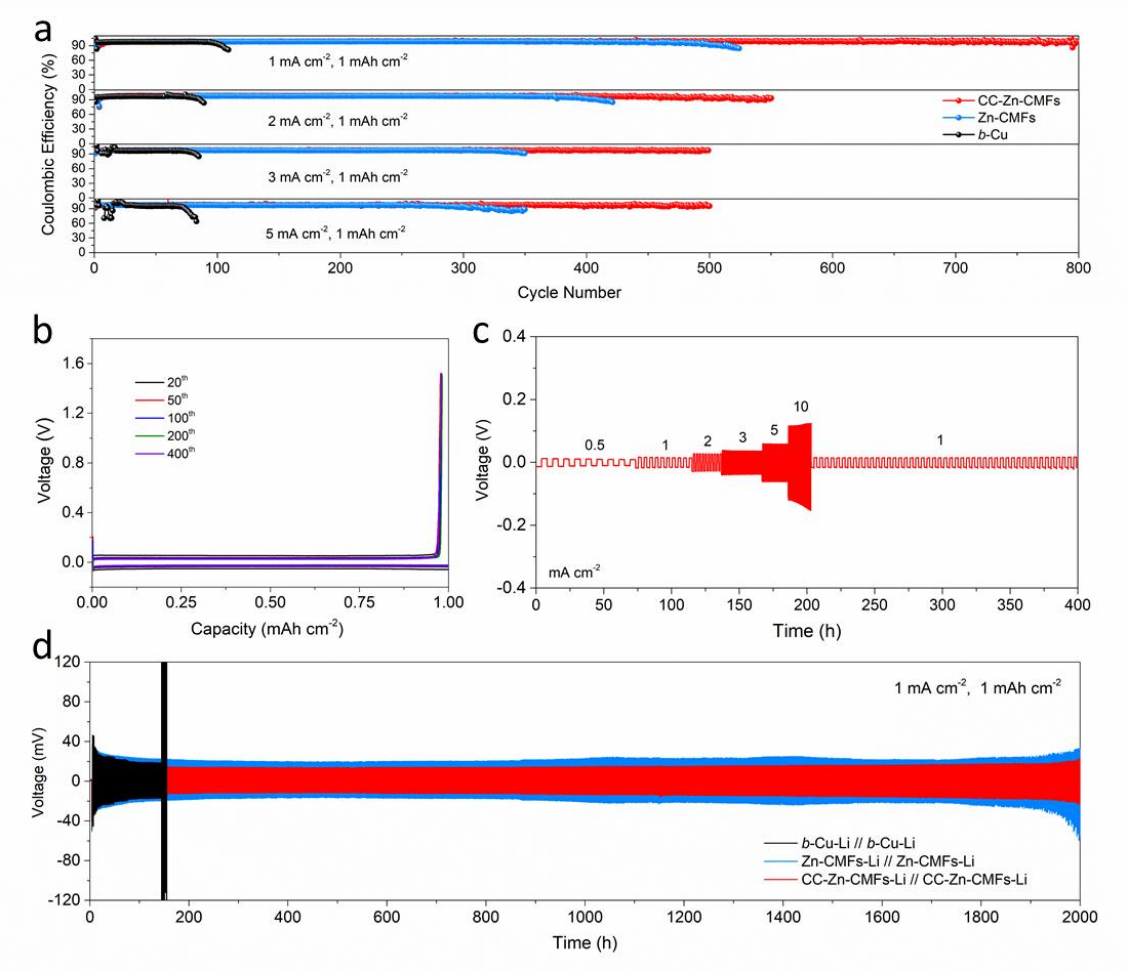

Figure 4. (a) CE of Li deposition on *b*-Cu, Zn-CMFs, and CC-Zn-CMFs at different current densities for the same capacity of 1 mAh cm^{-2}. (b) Selected electrochemical Li plating/stripping curves of the CC-Zn-CMFs electrode at 1 mA cm^{-2} for a capacity of 1 mAh cm^{-2}. (c) Rate performance of the CC-Zn-CMFs-Li anode in a symmetric cell at various current densities with a fixed capacity of 2 mAh cm^{-2}. (d) Galvanostatic cycling voltage profiles of *b*-Cu-Li, Zn-CMFs-Li, and CC-Zn-CMFs-Li anodes in symmetric cells at 1 mA cm^{-2} with a capacity of 1 mAh cm^{-2}.

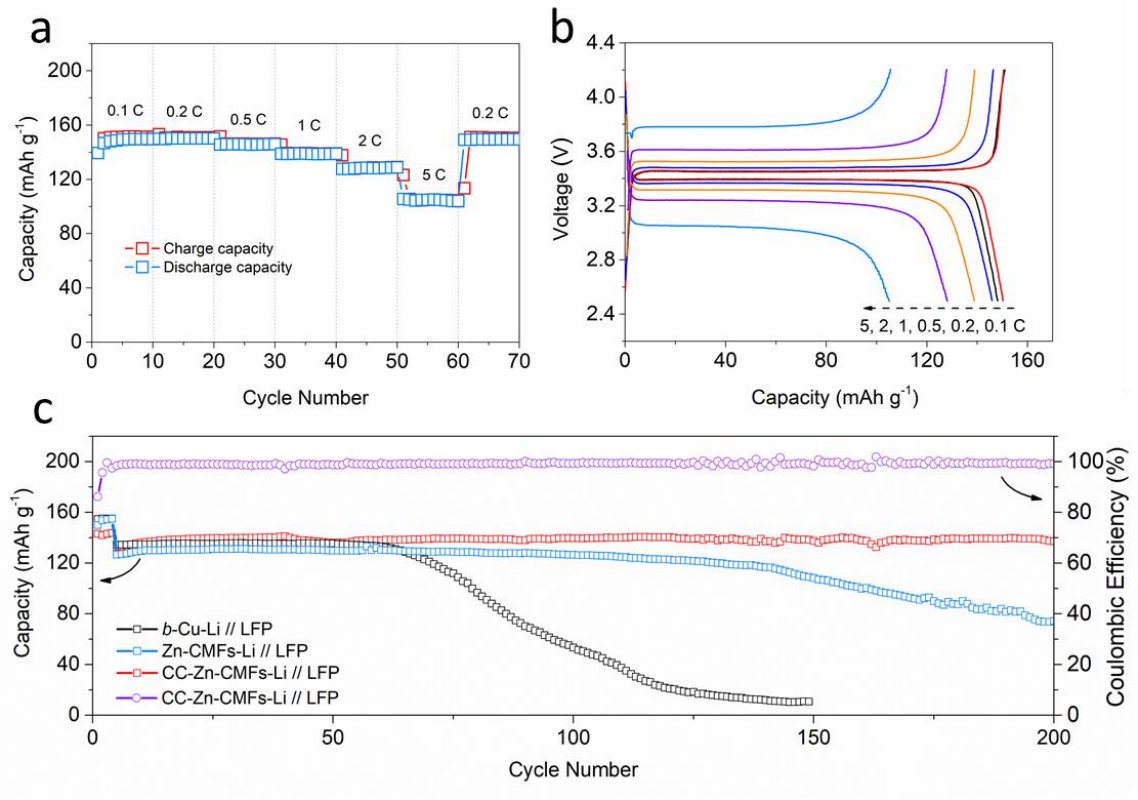

Figure 5. (a) Rate capability of the CC-Zn-CMFs-Li//LFP full cell. (b) The corresponding galvanostatic charge/discharge voltage curves of the CC-Zn-CMFs-Li//LFP full cell at different current rates. (c) Cycling stability of the *b*-Cu-Li//LFP, Zn-CMFs-Li//LFP, CC-Zn-CMFs-Li//LFP full cells at 1 C (1 C = 170 mA g^{-1}).

for Table of Content Entry

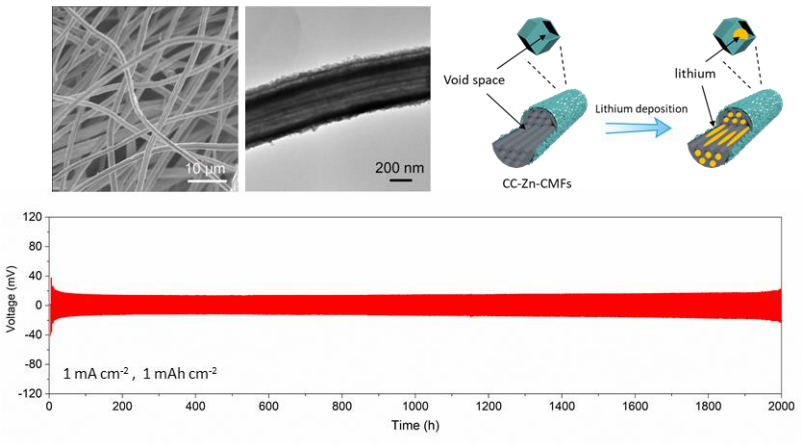

Carbon cages decorated nitrogen-doped amorphous Zn-carbon multichannel fibers (denoted as CC-Zn-CMFs) are synthesized as a multifunctional host for lithium metal anodes. With the unique hierarchical hollow architecture and functional composition, these CC-Zn-CMFs exhibit enhanced electrochemical properties for lithium metal anodes in terms of high Coulombic efficiency, superior rate capability, and long cycle life.